Knots as a Topological Order Parameter for Semiflexible Polymers

Martin Marenz* and Wolfhard Janke†
Institut für Theoretische Physik, Universität Leipzig, Postfach 100 920, D-04009 Leipzig, Germany
(Received 29 May 2015; revised manuscript received 31 July 2015; published 21 March 2016)

Using a combination of the multicanonical Monte Carlo algorithm and the replica-exchange method, we investigate the influence of bending stiffness on the conformational phases of a bead-stick homopolymer model and present the pseudophase diagram for the complete range of semiflexible polymers, from flexible to stiff. Although it is a simple model, we observe a rich variety of conformational phases, reminiscent of conformations observed for synthetic polymers or biopolymers. Depending on the bending stiffness, the model exhibits different pseudophases like bent, hairpin, or toroidal. In particular, we find thermodynamically stable knots and unusual transitions into these knotted phases with a clear phase coexistence, but almost constant mean total energy, and hence almost no latent heat.

DOI: 10.1103/PhysRevLett.116.128301

Since the first simulation of knotted polymers in 1975 [1], the occurrence and behavior of knots in polymers has been studied in various contexts. Scanning through protein data bases has revealed that several proteins form knots [2–4]. In particular, in 2006 Virnau *et al.* [5] reviewed the whole Protein Data Bank [6] and identified 36 proteins forming relatively simple knots. Today, many more knotted proteins are known [7], but still only a small fraction of proteins form knots—somehow evolution tries to avoid knotted proteins [8].

In contrast, flexible polymers form much more complicated knots by chance in the swollen [9–11] and globular [11,12] phases, which are present in models with self-avoidance and attraction of monomers, as already lattice polymer simulations show [13,14]. In this work we go a step ahead and investigate the knottedness of semiflexible bead-stick polymers. There exist a few studies concerning the more complex phase space of polymers governed by bending stiffness [15–17]. The most comprehensive work considered bead-spring polymers with finitely extensible nonlinear elastic (FENE) bonds [17]. Depending on the bending stiffness, these models are able to mimic a large class of polymers, exhibiting, for instance, bent, hairpin, or toroidal conformations.

Nevertheless, none of the former works considered the knottedness of a polymer over the full bending stiffness range, which we will discuss in this Letter. By measuring the knot type we found pseudophases [18] with thermodynamically stable knotted polymers. The knot type will be shown to be an ideal topological order parameter to identify the knotting transition and, moreover, the behavior at the transition from an unknotted to a knotted phase turns out to be surprisingly different from all other phase transitions of the bead-stick polymer in that it does not fit into the common classification scheme of first- and second-order phase transitions.

To model a coarse-grained polymer with an adjustable stiffness, we use a modified version of the bead-stick model of Refs. [19–21], which consists of N identical monomers connected by bonds with length 1. Nonadjacent monomers interact via the Lennard-Jones (LJ) potential

$$E_{\mathrm{LJ}} = 4\epsilon \sum_{i=1}^{N-2} \sum_{j=i+2}^{N} \left[\left(\frac{\sigma}{r_{ij}}\right)^{12} - \left(\frac{\sigma}{r_{ij}}\right)^{6} \right], \tag{1}$$

where r_{ij} is the distance between two monomers. The parameters ϵ and σ are set to 1 for the rest of this work, i.e., energies are measured in units of ϵ and lengths in units of σ. The stiffness is introduced through the cosine potential adopted from the well-known discretized worm-like chain model [22] and defined by

$$E_{\mathrm{bend}} = \sum_{i=1}^{N-2} (1 - \cos\theta_i), \tag{2}$$

where θ_i represents the angle between adjacent bonds. The complete Hamiltonian is then given by $E = E_{\mathrm{LJ}} + \kappa E_{\mathrm{bend}}$, where κ parametrizes the strength of the bending term compared to the LJ potential.

Topological barriers between the knotted phases forced us to apply relatively complex Monte Carlo (MC) algorithms in order to obtain reliable results. To simulate the system in the complete (T, κ) plane, we used two complementary MC algorithms. The first is a combination of the (parallelized) multicanonical (MUCA) method [23,24] and a replica exchange (RE) [25] in the κ direction (MUCA + RE). This means that we run m individual MUCA simulations, each at a different value for κ. Within RE the canonical Boltzmann factors in the usual acceptance probability are replaced with the multicanonical weights obtained from the MUCA method. The second variant is a two-dimensional version of the replica-exchange (2D RE) method, which runs standard Metropolis MC simulations at m different parameter pairs (T, κ). By means of a two-dimensional weighted

histogram analysis method [26], we are able to calculate the canonical mean values of observables at any point in the (T, κ) plane within the simulated parameter ranges in arbitrarily high resolution. Statistical errors are computed with the jackknife method [27]. To generate well equilibrated results it was necessary to apply bridge-end and double-bridging moves [28], which are modified such that they respect the fixed bond-length constraint, besides the common crank-shaft, spherical-rotation, and pivot moves. As a useful cross-check, we performed the simulations with both methods, MUCA + RE and 2D RE, and confirmed that the results are in good agreement with each other. For recent reviews of these technical aspects, see Refs. [29,30] and the Supplemental Material [31].

To determine the structural phases, we measured the total energy $\langle E \rangle$, both subenergies $\langle E_{\mathrm{LJ}} \rangle$ and $\langle E_{\mathrm{bend}} \rangle$, the squared end-to-end distance $\langle R_{\mathrm{ee}}^2 \rangle$, the squared radius of gyration $\langle R_g^2 \rangle$, and the eigenvalues of the gyration tensor $\langle \lambda_1 \rangle$, $\langle \lambda_2 \rangle$, $\langle \lambda_3 \rangle$. Peaks of their derivatives with respect to temperature for a given κ mark the locations of the different phase transitions. Additionally, we performed microcanonical analyses [32] as a complementary approach to identify the different phase transitions. These are based on the microcanonical entropy $S(E) = k_B \ln \Omega(E)$ and the inverse temperature $\beta_{\mathrm{micro}}(E) = dS(E)/dE$, where $\Omega(E)$ is the density of states. A peak in the derivative $d\beta_{\mathrm{micro}}(E)/dE$ signals a phase transition.

To identify the knots, we determined the knot type of the polygonal line defined by the polymer. In principle, the knot type, denoted by C_n, defines which smooth closed curves can be transformed into each other by applying multiple Reidemeister moves. Practically, this means two knots are not of the same type if they cannot be deformed into each other without cutting and rejoining the polygonal line. The integer number C counts the minimal number of crossings for any projection on a plane and the subscript n distinguishes topologically different knots with the same number of crossings. A detailed exposition of mathematical knot theory can be found in Ref. [33]. Of course, an open polymer cannot satisfy the mathematical definition of a knot, unless the termini are closed virtually. The closure is only applied during the measurement of the knot type and does not influence the simulation itself. We used a closure that pulls the two termini in opposite directions and connects them outside the polymer as inspired by tying a real knot, see the Supplemental Material [31] for detailed instructions. In Refs. [11,34] it is documented that a reasonably constructed closure should have no significant influence on the found knots. In fact, in our own tests with other closures we confirmed this claim [31]. To calculate the knot type C_n, we employed a technique described in Ref. [34], which is based on a variant of the Alexander polynomial $\Delta(t)$,

$$\Delta_p(t) = |\Delta(t) \times \Delta(1/t)|, \tag{3}$$

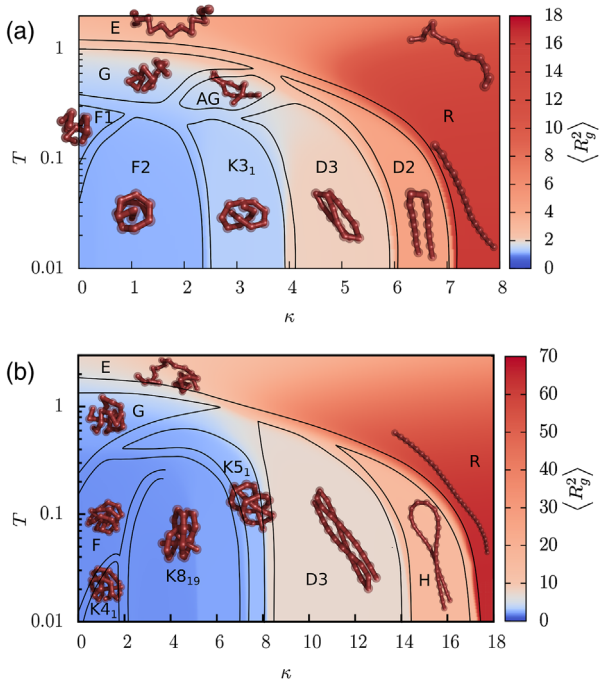

FIG. 1. Phase diagram for (a) 14 and (b) 28 monomers. The black transition lines sum up all signals of the thermally most active regions. The surface plot shows the average size of the polymer in terms of $\langle R_g^2 \rangle$. The phases are labeled as follows: E, elongated; R, rodlike; G, globular (AG is an artifact of the small chain length; both termini of the polymer are aligned); F, frozen; KC_n, knotted phase with the corresponding knot type; DN, $(N-1)$ times bent polymers; H, hairpin. We omitted some subphases of DN, K8$_{19}$, and F, which do not change the overall picture.

evaluated at $t = -1.1$. Strictly speaking, the Alexander polynomial and likewise $D \equiv \Delta_p(-1.1)$ are not unique invariants. However, the value for D is unique for all knots found in this work and thus characterizes topologically different polymer conformations.

In the simulations we considered chains with $N = 14$ and 28 monomers, which is motivated by the length range of recent experiments [35,36]. The stiffness-dependent behavior of our bead-stick model defined by (1) and (2) is summed up in the phase diagrams shown in Fig. 1, which are constructed from the peaks of all measured thermal derivatives and the results of the microcanonical analysis. The black lines mark the thermally most active regions and represent the location of the phase transitions. Estimates from different observables give slightly different transition temperatures, due to the finite length of the polymer. Therefore, the space between the black lines reflects this variance. The color map encodes the average extension of the polymer in terms of $\langle R_g^2 \rangle$. For high temperatures, where the system is entropy dominated and the polymer resembles a discretized wormlike chain, the conformations are either gaseouslike and extended (E) or rodlike (R). When the temperature is lowered, the LJ energy becomes more

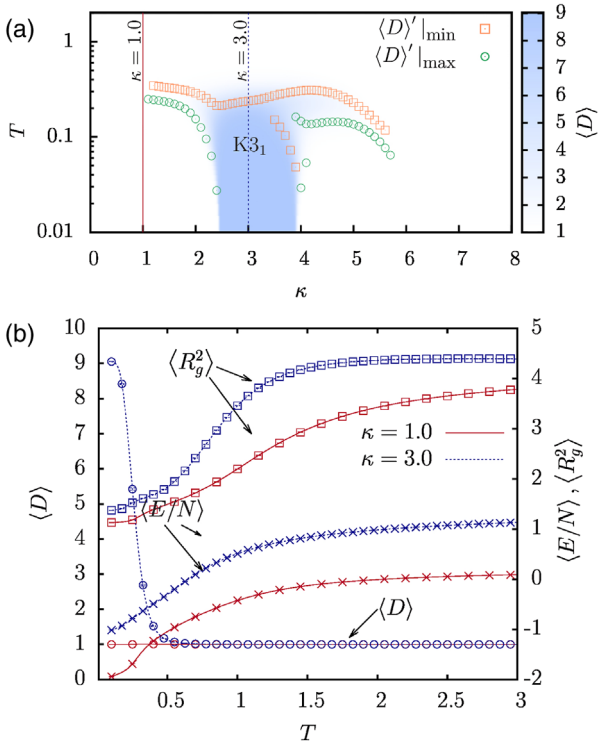

FIG. 2. (a) Surface plot of $\langle D\rangle$ for a 14-mer over the same (T, κ) range as in Fig. 1(a). The blue regime, $\langle D\rangle = 9.05463$, marks the $K3_1$ knot phase. The orange squares and green circles are the positions of the minima and maxima of $\langle D\rangle'$. The two vertical lines mark the κ values for which in (b) the temperature profiles of $\langle R_g^2\rangle$, $\langle E/N\rangle$, and $\langle D\rangle$ are shown. The lines are obtained with the weighted histogram analysis method. The statistical accuracy is indicated by the data symbols with error bars, which are of the order of the line width.

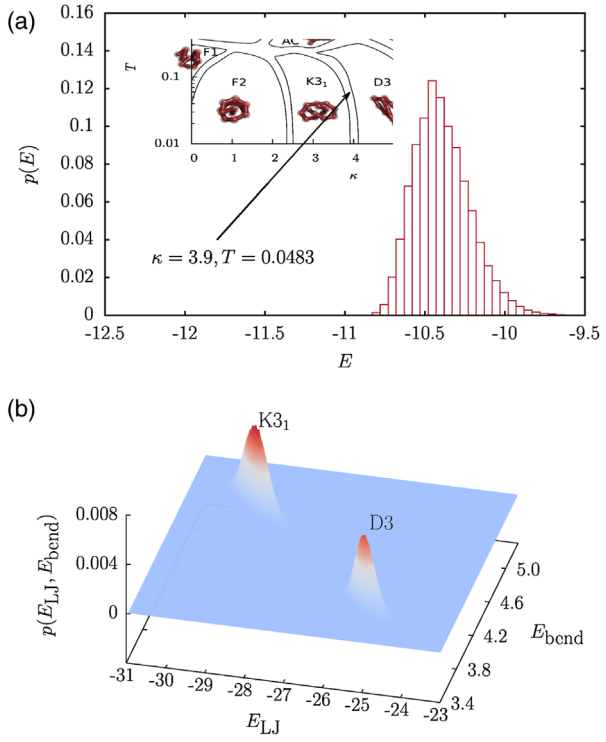

FIG. 3. (a) Energy probability distribution $p(E)$ of a 14-mer at $\kappa = 3.9$, $T = 0.0483$ where $\langle D\rangle'$ suggests a knotting transition as indicated in the inset. In (b) the energy is split into the two subenergies, which reveal the double peak in the two-dimensional probability distribution $p(E_{LJ}, E_{bend})$, reflecting the knotted state $K3_1$ and the bent state D3. $p(E)$ is exactly the projection of $p(E_{LJ}, E_{bend})$ along the line connecting the two peaks; thus, the phase coexistence is perfectly hidden in $p(E)$.

important and the polymer collapses. One can clearly distinguish two different regimes. For small κ, the polymer behaves similarly to a flexible chain and undergoes a continuous phase transition into the globular (G) phase, which is comparable to a liquid where individual monomers are located close to each other but move relative freely. Upon further lowering the temperature, in a first-order-like transition, it enters frozen (F) states where the distances between the monomers become minimized and different crystallike conformations occur, e.g., the 14-mer exhibits in F2 a more pronounced core than in F1. This contrasts with larger κ, where the polymer undergoes a first-order-like transition from the rodlike (R) states to states with differently structured motifs (DN, H, KC_n). The notion "first-order-like" is again a caution in that for finite systems the Ehrenfest classification is not strictly applicable but we nevertheless observe phase coexistence and signals in the microcanonical analysis as for "real" first-order transitions. For clarity, we omitted in Fig. 1 some subphases where the shape parameters and microcanonical analysis suggest additional transitions between differently shaped conformations of the same motif. Especially, the frozen phase F subsumes many subphases, which differ only in minor aspects.

In the knotted phases KC_n the probability to find the corresponding knot is almost 1. This means every polymer chain is of that specific knot type and implies that the knots are thermodynamically stable. We want to emphasize that this is different from the knots found in previous work, which occur in the swollen and globular phases of flexible polymers and form by chance. This makes $\langle D\rangle$ a perfect topological order parameter to distinguish knotted and unknotted phases, as is demonstrated in Fig. 2(a) for a 14-mer. We use the minima and maxima of the temperature derivative $\langle D\rangle' \equiv d\langle D\rangle/dT$ to confirm the phase boundaries. In Fig. 2(b) one can see that the behavior of $\langle E/N\rangle$ and $\langle R_g^2\rangle$ is qualitatively not very different at the freezing transition G $\leftrightarrow$ F2 ($\kappa = 1.0$) and the knotting transition AG $\leftrightarrow$ $K3_1$ ($\kappa = 3.0$). The knot parameter $\langle D\rangle$, however, clearly signals the phase transition and goes from 1 (unknotted polymer) to 9.05463 (3_1 knot) only in the case of a transition into a stable knot. As expected, the 28-mer (and even more the 42-mer [37]) exhibits a richer phase diagram with more complicated knot types, see Fig. 1(b). However, the qualitative behavior at the phase boundaries

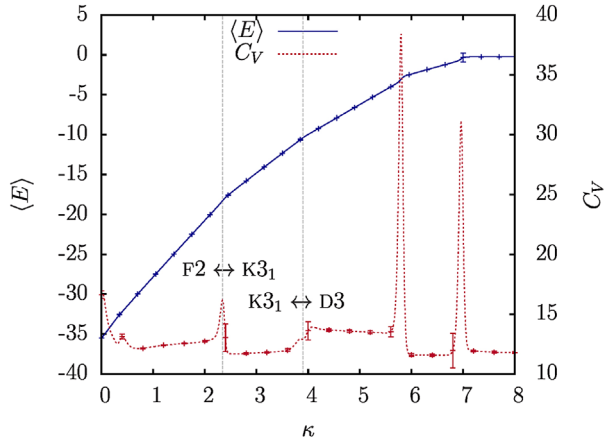

FIG. 4. Mean total energy $\langle E\rangle$ and heat capacity C_V of a 14-mer at $T = 0.0483$. At both knotting transitions, $\kappa = 2.36$ (F2 $\leftrightarrow$ $K3_1$) and $\kappa = 3.9$ ($K3_1 \leftrightarrow$ D3), we found no significant shift in the energy and therefore no signal in C_V that is larger than the statistical error. The lines are obtained with the weighted histogram analysis method. The statistical accuracy is indicated by the data symbols with error bars.

turned out to be very similar so that we will focus in the following discussion on the 14-mer.

The knotting transitions from one structured state to another (e.g., $K3_1 \leftrightarrow$ D3) are quite intriguing. At first glance, one could assume that they behave first-order-like, similar to other solid-solid-like transitions at low temperatures. However, the microcanonical analysis exhibits no convex intruder in the microcanonical entropy that would indicate a first-order-like transition. Likewise, the canonical probability distribution $p(E)$ does not exhibit a double-peak structure, see Fig. 3(a). On the other hand, the two-dimensional energy distribution $p(E_{\mathrm{LJ}}, E_{\mathrm{bend}})$ points to a phase coexistence. In Fig. 3(b) one can clearly identify two separate peaks, one corresponding to the knotted phase and the other to the unknotted phase. Surprisingly, both phases have almost identical mean total energy $\langle E\rangle$ at the coexistence point, and there is almost no signal in $\langle E\rangle$ and the heat capacity $C_V = d\langle E\rangle/dT$ at the transition, see Fig. 4. We thus observe almost no latent heat when the polymer undergoes the transition into the knotted phase. Rather, the LJ energy and the bending energy are transformed into each other [38].

This behavior changes if the polymer enters the knotted phase from an unstructured conformation (e.g., AG $\leftrightarrow$ $K3_1$). For example, crossing the transition line $K3_1 \leftrightarrow$ D3 of the 14-mer for fixed κ at higher temperatures, the two peaks in $p(E_{\mathrm{LJ}}, E_{\mathrm{bend}})$ start to merge until they form a single peak at the transition AG $\leftrightarrow$ $K3_1$ and the phase coexistence vanishes. It seems that in that case the transition into the knot is a continuous one. This holds for all investigated knotting transitions; the transitions from a structured (F, DN, KC_n) to a knotted phase exhibit phase coexistence, whereas the transitions from an unstructured (G, AG) to a knotted phase seem to be continuous.

The reason for the missing knotted phases in Ref. [17] is not rooted in this intricate behavior with "concealed" signals, however, but may rather lie in the choice of the bond length r_b and the minimum distance r_{min} of the LJ potential to coincide, whereas they differ by a factor of 1.12 in our work. Test simulations of their model and other common parametrizations [39] of bead-spring models suggest that the regions of thermodynamically stable knots are much smaller when $r_b \approx r_{\mathrm{min}}$. The observation that the polymer minimizes its total energy in bent conformations by maximizing the number of monomers located in the LJ minima leads to the following conjecture: if $r_b \approx r_{\mathrm{min}}$ and the bonds are flexible enough, bent conformations are energetically so strongly favored that knotted states become unlikely.

In conclusion, we have investigated the complete stiffness-dependent behavior of a semiflexible bead-stick polymer. Besides the conformations already observed in previous work, we found phase transitions into novel phases with knots as the predominant conformation. These are considerably different from the knots observed in the swollen or globular phase of flexible polymers, which form by chance, whereas the here found knots are thermodynamically stable. We showed that $\langle D\rangle$ is a perfect topological order parameter to distinguish them. The second intriguing observation is that the transitions into these knotted states from other structured conformations happen with almost no latent heat, although we observed a clear phase coexistence. Interestingly, most of the found knots in this work ($3_1, 5_1, 8_{19}$) are so-called torus knots, which are known to be formed preferentially in viral DNA [40,41]. A further investigation of this connection may be illuminating.

At the moment, investigating short single polymer chains in experiments seems unrealistic, and it appears even more unrealistic to observe structural properties such as knots. However, preparation and detection methods for single polymers at surfaces have recently made quite impressive progress [35,36], so that one can now resolve polymers of down to 20 monomers. A sensible next step could be hence an investigation of the influence of an adsorbing surface on the occurrence of stable knotted phases for a generic semiflexible polymer. Later on, this could be extended to more realistic synthetic polymer models to guide experiments.

We would like to thank Johannes Zierenberg, Niklas Fricke, Stefan Schnabel, Jan Meischner, and Martin Treffkorn for many fruitful discussions. Computing time provided by the John von Neumann Institute for Computing (NIC) under Grant No. HLZ21 on the supercomputer JUROPA at Jülich Supercomputing Centre (JSC) is gratefully acknowledged. This project has been funded by the European Union and the Free State of Saxony through the "Sächsische AufbauBank" and by the DFG (German Science Foundation) through SFB/TRR 102 (project B04) and the Graduate School GSC 185 "BuildMoNa."

*martin.marenz@itp.uni-leipzig.de
†wolfhard.janke@itp.uni-leipzig.de

[1] M. Frank-Kamenetskii, A. Lukashin, and A. Vologodskii, Statistical mechanics and topology of polymer chains, Nature (London) **258**, 398 (1975).
[2] M. L. Mansfield, Are there knots in proteins?, Nat. Struct. Biol. **1**, 213 (1994).
[3] W. R. Taylor, A deeply knotted protein structure and how it might fold, Nature (London) **406**, 916 (2000).
[4] R. C. Lua and A. Y. Grosberg, Statistics of knots, geometry of conformations, and evolution of proteins, PLoS Comput. Biol. **2**, e45 (2006).
[5] P. Virnau, L. A. Mirny, and M. Kardar, Intricate knots in proteins: Function and evolution, PLoS Comput. Biol. **2**, e122 (2006).
[6] H. M. Berman, J. Westbrook, Z. Feng, G. Gilliland, T. N. Bhat, H. Weissig, I. N. Shindyalov, and P. E. Bourne, The Protein Data Bank, Nucleic Acids Res. **28**, 235 (2000); http://www.pdb.org.
[7] M. Jamroz, W. Niemyska, E. J. Rawdon, A. Stasiak, K. C. Millett, P. Sułkowski, and J. I. Sulkowska, KnotProt: A database of proteins with knots and slipknots, Nucleic Acids Res. **43**, D306 (2015).
[8] T. Wüst, D. Reith, and P. Virnau, Sequence Determines Degree of Knottedness in a Coarse-grained Protein Model, Phys. Rev. Lett. **114**, 028102 (2015).
[9] K. Koniaris and M. Muthukumar, Knottedness in Ring Polymers, Phys. Rev. Lett. **66**, 2211 (1991).
[10] T. Deguchi and K. Tsurusaki, Universality of random knotting, Phys. Rev. E **55**, 6245 (1997).
[11] P. Virnau, Y. Kantor, and M. Kardar, Knots in globule and coil phases of a model polyethylene, J. Am. Chem. Soc. **127**, 15102 (2005).
[12] R. Lua, A. L. Borovinskiy, and A. Y. Grosberg, Fractal and statistical properties of large compact polymers: A computational study, Polymer **45**, 717 (2004).
[13] U. Bastolla and P. Grassberger, Phase transitions of single semistiff polymer chains, J. Stat. Phys. **89**, 1061 (1997).
[14] J. Krawczyk, A. L. Owczarek, and T. Prellberg, A semiflexible attracting segment model of two-dimensional polymer collapse, Physica (Amsterdam) **389A**, 1619 (2010).
[15] H. Noguchi and K. Yoshikawa, First-order phase transition in a stiff polymer chain, Chem. Phys. Lett. **278**, 184 (1997).
[16] V. A. Ivanov, W. Paul, and K. Binder, Finite chain length effects on the coil-globule transition of stiff-chain macromolecules: A Monte Carlo simulation, J. Chem. Phys. **109**, 5659 (1998).
[17] D. T. Seaton, S. Schnabel, D. P. Landau, and M. Bachmann, From Flexible to Stiff: Systematic Analysis of Structural Phases for Single Semiflexible Polymers, Phys. Rev. Lett. **110**, 028103 (2013).
[18] The notion "pseudo-" phase indicates that strictly speaking a phase and the corresponding phase transition are only well defined in the thermodynamic limit (number of monomers $N \to \infty$). Most of the here described pseudo-phases depend on N. Nevertheless, they still determine the behavior of mesoscopic systems. We neglect pseudo in the following.
[19] F. H. Stillinger, T. Head-Gordon, and C. L. Hirshfeld, Toy model for protein folding, Phys. Rev. E **48**, 1469 (1993).
[20] A. Irbäck, C. Peterson, F. Potthast, and O. Sommelius, Local interactions and protein folding: A three-dimensional off-lattice approach, J. Chem. Phys. **107**, 273 (1997).
[21] M. Bachmann, H. Arkin, and W. Janke, Multicanonical study of coarse-grained off-lattice models for folding heteropolymers, Phys. Rev. E **71**, 031906 (2005).
[22] M. Rubinstein and R. H. Colby, *Polymer Physics* (Oxford University Press, Oxford, 2003).
[23] B. A. Berg and T. Neuhaus, Multicanonical algorithms for first order phase transitions, Phys. Lett. B **267**, 249 (1991); Multicanonical Ensemble: A New Approach to Simulate First-order Phase Transitions, Phys. Rev. Lett. **68**, 9 (1992).
[24] J. Zierenberg, M. Marenz, and W. Janke, Scaling properties of a parallel implementation of the multicanonical algorithm, Comput. Phys. Commun. **184**, 1155 (2013).
[25] K. Hukushima and K. Nemoto, Exchange Monte Carlo method and application to spin glass simulations, J. Phys. Soc. Jpn. **65**, 1604 (1996).
[26] A. M. Ferrenberg and R. H. Swendsen, New Monte Carlo Technique for Studying Phase Transitions, Phys. Rev. Lett. **61**, 2635 (1988); **63**, 1658(E) (1989); Optimized Monte Carlo Data Analysis, Phys. Rev. Lett. **63**, 1195 (1989); S. Kumar, J. Rosenberg, D. Bouzida, R. H. Swendsen, and P. Kollman, The weighted histogram analysis method for free-energy calculations on biomolecules. I. The method, J. Comput. Chem. **13**, 1011 (1992).
[27] B. Efron, *The Jackknife, the Bootstrap, and Other Resampling Plans* (Society for Industrial and Applied Mathematics, Philadelphia, 1982).
[28] S. Schnabel, W. Janke, and M. Bachmann, Advanced multicanonical Monte Carlo methods for efficient simulations of nucleation processes of polymers, J. Comput. Phys. **230**, 4454 (2011).
[29] *Rugged Free Energy Landscapes Common Computational Approachess to Spin Glasses, Structural Glasses and Biological Macromolecules*, edited by W. Janke, Lect. Notes Phys. Vol. 736 (Springer, Berlin, 2008).
[30] W. Janke and W. Paul, Thermodynamics and structure of macromolecules from flat-histogram Monte Carlo simulations, Soft Matter **12**, 642 (2016).
[31] See Supplemental Material at http://link.aps.org/supplemental/10.1103/PhysRevLett.116.128301 for a more detailed description of the methods used to generate and analyze the data.
[32] C. Junghans, M. Bachmann, and W. Janke, Microcanonical Analyses of Peptide Aggregation Processes, Phys. Rev. Lett. **97**, 218103 (2006).
[33] L. H. Kauffman, *Knots and Physics*, 2nd ed. (World Scientific, Singapore, 1991).
[34] P. Virnau, Detection and visualization of physical knots in macromolecules, Phys. Procedia **6**, 117 (2010).
[35] S. Förster and W. Widdra, Structure of single polythiophene molecules on Au(001) prepared by in situ UHV electrospray deposition, J. Chem. Phys. **141**, 054713 (2014).
[36] S. Förster, E. Kohl, M. Ivanov, J. Gross, W. Widdra, and W. Janke, Polymer adsorption on reconstructed Au(001): A statistical description of P3HT by scanning tunneling microscopy and coarse-grained Monte Carlo simulations, J. Chem. Phys. **141**, 164701 (2014).

[37] Not shown here, because the details of the more complicated phase diagram do not contribute to the understanding of the basic mechanism.

[38] This topological change also explains why we need the MUCA + RE or 2D RE algorithm to overcome the topological barrier.

[39] For the LJ potential we use here $\epsilon = 1, \sigma = 2^{-1/6}$ so that $r_{\min} = 1$, and the stiff bonds are replaced by FENE springs, $E_{\mathrm{FENE}} = -(K/2)R^2 \ln(1 - [(r - r_b)/R]^2)$, with $K = 40, R = 0.3, r_b = 1$ and $K = 60, R = 0.1, r_b = 1.3$.

[40] J. Arsuaga, M. Vazquez, P. McGuirk, S. Trigueros, D. W. Sumners, and J. Roca, DNA knots reveal a chiral organization of DNA in phage capsids, Proc. Natl. Acad. Sci. U.S.A. **102**, 9165 (2005).

[41] D. Reith, P. Cifra, A. Stasiak, and P. Virnau, Effective stiffening of DNA due to nematic ordering causes DNA molecules packed in phage capsids to preferentially form torus knots, Nucleic Acids Res. **40**, 5129 (2012).